A Concept for the Synthesis of 3-Dimensional Homo- and Bimetallic Oxalate-Bridged Networks $[M_2(ox)_3]_n$. Structural, Mössbauer, and Magnetic Studies in the Field of Molecular-Based Magnets

Silvio Decurtins,*,† Helmut W. Schmalle,† Philippe Schneuwly,† Jürgen Ensling,‡ and Philipp Gütlich‡

Contribution from the Institut für Anorganische Chemie, Universität Zürich, Winterthurerstrasse 190, CH-8057 Zürich, Switzerland, and Institut für Anorganische Chemie und Analytische Chemie, Johannes Gutenberg-Universität Mainz, Staudingerweg 9, D-55099 Mainz, Germany

Received February 3, 1994®

Abstract: The tris-chelated $[M^{II}(bpy)_3]^{2+}$ cations, where M^{II} is a divalent transition metal and bpy is 2,2′-bipyridine, cause a remarkable crystallization of anionic three-dimensional (3D) coordination polymers of oxalate-bridged metal complexes $[M_2(ox)_3]_n^{2n-}$. With these cations, which are appropriate in charge, size, and symmetry, two types of stoichiometric units of the anionic 3D networks, with metals in different valence states, can be distinguished: $[M^{II}_2(ox)_3]^{2-}$ and $[M^{I}M^{III}(ox)_3]^{2-}$. Results of a structural analysis of compounds within each of the two isomorphous series are discussed: $[Ni^{II}(bpy)_3][Mn^{II}_2(ox)_3]$ (**3**), cubic, merohedrically twinned, $P4_132/P4_332$, a = 15.579(2) Å, Z = 4; $[Fe^{II}(bpy)_3][NaFe^{III}(ox)_3]$ (**4**), cubic, $P2_13$, a = 15.507(3) Å, Z = 4; $[Fe^{II}(bpy)_3][LiCr^{III}(ox)_3]$ (**5**), cubic, $P2_13$, a = 15.262(4) Å, Z = 4. The Mössbauer spectra of the iron-containing compounds $[Fe^{II}(bpy)_3][Fe^{II}_2(ox)_3]$ (**1**) and $[Fe^{II}(bpy)_3][Mn^{II}_2(ox)_3]$ (**2**) and type **4** but $LiFe^{III}$ are consistent with the stoichiometric formula and the corresponding iron valence states. The straightforward synthetic approach and easy crystallization behavior, as well as the variety of metal combinations within the 3D networks, render these systems valuable candidates for studies in the field of molecular-based magnets. They fulfill the requirements of three-dimensional connectivity as well as accessibility to detailed structural characterization. The magnetic susceptibility data in the temperature range 2–300 K of **1**, **2** and type **4** but $LiFe^{III}$ are presented and the results should be taken as a starting point for more extended systematical studies. **1** and **2** reveal antiferromagnetic ordering behavior, indicated by a negative Weiss constant θ of −28 and −33 K, whereas the $LiFe^{III}$ compound exhibits the expected behavior of single iron(III) ions. Further extensions to possible networks of the types $[M^{II}M^{III}(ox)_3]_n^{1n-}$ and $[M^{I}M^{II}(ox)_3]_n^{3n-}$ are discussed.

Introduction

The field of molecular-based magnets has received considerable interest in the past few years.[1-3] Up to now, several coordination compounds,[4-11] metal–radical complexes,[12-17] and pure organic compounds[18,19] have been shown to exhibit spontaneous magnetization; however the critical temperatures (T_c) are found to be almost exclusively in the liquid helium temperature range. In the few cases where higher T_c values are present, e.g. between 90 and 240 K[6,7] or even when room temperature is exceeded,[17] a chemically linked three-dimensional (3D) network of the spin carriers is thought to be the origin, although the detailed structural verifications are not yet available.

This concise summary focuses directly on the decisive factors affecting the molecular design of magnetic materials. On one side it is called the problem of dimensionality, and on the other side there is the declared need for accurate structural data for those solids exhibiting cooperative magnetic phenomena. The former aspect deals with the question of how to achieve the three-dimensional magnetic ordering. For chemically linked one- and two-dimensional systems, above all, the complementary intermolecular interactions have to be controlled. However, these intermolecular interactions are in general very weak and as a result the critical temperature, T_c, is limited to low temperatures. If the underlying structure is built up from a chemically linked three-dimensional network, the shortcomings due to the weak intermolecular interactions could be excluded. Without doubt,

* Author to whom correspondence should be addressed.
† Institut für Anorganische Chemie, Universität Zürich.
‡ Institut für Anorganische Chemie und Analytische Chemie, Universität Mainz.
® Abstract published in *Advance ACS Abstracts*, September 1, 1994.

(1) *Proceedings of the Symposium on Ferromagnetic and High Spin Molecular Based Materials*; Miller, J. S., Dougherty, D. A., Eds.; Molecular Crystals and Liquid Crystals, No. 176; Gordon & Breach: London, 1989.
(2) Gatteschi, D.; Kahn, O.; Miller, J. S.; Palacio, F. *Magnetic Molecular Materials*; NATO ASI Series; Kluwer: The Netherlands, Dordrecht, 1991.
(3) *Proceedings of the International Symposium on Chemistry and Physics of Molecular Based Magnetic Materials*; Iwamura, H., Itoh, K., Kinoshita, M., Eds.; Molecular Crystal and Liquid Crystals: Gordon & Breach: London, 1993.
(4) Stumpf, H. O.; Pei, Y.; Kahn, O.; Sletten, J.; Renard, J. P. *J. Am. Chem. Soc.* **1993**, *115*, 6738.
(5) Stumpf, H. O.; Ouahab, L.; Pei, Y.; Grandjean, D.; Kahn, O. *Science* **1993**, *261*, 447.
(6) Gadet, V.; Mallah, T.; Castro, I.; Verdaguer, M. *J. Am. Chem. Soc.* **1992**, *114*, 9213.
(7) Mallah, T.; Thiébaut, S.; Verdaguer, M.; Veillet, P. *Science* **1993**, *262*, 1554.
(8) Tamaki, H.; Zhong, Z. J.; Matsumoto, N.; Kida, S.; Koikawa, M.; Achiwa, N.; Hashimoto, Y.; Okawa, H. *J. Am. Chem. Soc.* **1992**, *114*, 6974.
(9) Ohba, M.; Tamaki, H.; Matsumoto, N.; Okawa, H. *Inorg. Chem.* **1993**, *32*, 5385.
(10) Sapina, F.; Burgos, M.; Escriva, E.; Folgado, J.-V.; Marcos, D.; Beltran, A.; Beltran, D. *Inorg. Chem.* **1993**, *32*, 4337.
(11) Decurtins, S.; Schmalle, H. W.; Oswald, H. R.; Linden, A.; Ensling, J.; Gütlich, P.; Hauser, A. *Inorg. Chim. Acta* **1994**, *216*, 65.
(12) Caneschi, A.; Gatteschi, D.; Rey, P.; Sessoli, R. *Inorg. Chem.* **1991**, *30*, 3936.
(13) Benelli, C.; Caneschi, A.; Gatteschi, D.; Sessoli, R. *Inorg. Chem.* **1993**, *32*, 4797.
(14) Oshio, H. *Inorg. Chem.* **1993**, *32*, 4123.
(15) Miller, J. S.; Zhang, J. H.; Reiff, W. M. *J. Am. Chem. Soc.* **1987**, *109*, 4584.
(16) Yee, G. T.; Manriquez, J. M.; Dixon, D. A.; McLean, R. S.; Groski, D. M.; Flippen, R. B.; Narayan, K. S.; Epstein, A. J.; Miller, J. S. *Adv. Mater.* **1991**, *3*, 309.
(17) Manriquez, J. M.; Yee, G. T.; McLean, R. S.; Epstein, A. J.; Miller, J. S. *Science* **1991**, *252*, 1415.
(18) Chiarelli, R.; Novak, M. A.; Rassat, A.; Tholence, J. L. *Nature* **1993**, *363*, 147.
(19) Jacobs, S. J.; Shultz, D. A.; Jain, R.; Novak, J.; Dougherty, D. A. *J. Am. Chem. Soc.* **1993**, *115*, 1744.

0002-7863/94/1516-9521$04.50/0

such attempts need to be coupled with detailed structural analyses since this is a prerequisite for the study and an understanding of the magnetic behavior.

From this viewpoint, the reports of the magnetic properties of oxalate-bridged polymeric metal assemblies,[8,11] although structurally two-dimensional, bear significant and basic data, which can be utilized for extension to analogous three-dimensional structures. The structural verification of just such as 3D oxalate-bridged metal complex has recently been reported and involves the photochemical synthesis of $[Fe(bpy)_3][Fe_2(ox)_3]$.[20] A search for alternative synthetic approaches toward these three-dimensional complexes while allowing the possibility of systematically varying the metal ions has now been successfully achieved in a remarkable straightforward way.

In this report we describe conceptually the synthetic possibilities for building up 3D oxalate-bridged metal networks and discuss their structural analyses. Mössbauer data on iron-containing compounds complement the analytical characterization. Besides the structural discussion, the magnetic properties are of paramount interest and the magnetic susceptibilities of the Fe(II) and Mn(II) networks are presented. These magnetic data, which at this stage are not yet fully understood, represent a starting point for a systematic study on different systems. Further experiments will focus mainly on the magnetic properties and will attempt to answer the following question. Does the characteristic connectivity within these 3D 10-gon networks lead to unusual or unexpected spin alignments which are inherently bound to the topology of the nets, or do different metal combinations lead to quite different magnetic properties? In any respect, these systems represent valuable case studies, particularly in the field of molecular-based magnets.

Although this report will concentrate on the structural and preliminary magnetic characterization of two types of networks, namely $[M^{II}_2(ox)_3]_n^{2n-}$ and $[M^{I}M^{III}(ox)_3]_n^{2n-}$, very recent data, which will be discussed in the concluding remarks, demonstrate the flexibility of the systems in that they are also extendable to e.g. $[M^{II}M^{III}(ox)_3]_n^{1n-}$ type nets. Of course, in the light of their magnetic properties, exact structural data and magnetic experiments of an alternating M^{II}–M^{III} system will also be of significant interest.

Experimental Section

Materials. The $[M^{II}(bpy)_3]^{2+}$ cations (as chloride or sulfate salts) and $K_3[M^{III}(ox)_3]\cdot 3H_2O$ were prepared according to the literature methods.[21,22] The other chemicals are commercially available and were used as purchased. For the incorporation of metal(I) or metal(II) ions into the oxalate-bridged networks, the corresponding chloride, nitrate, or sulfate salts were used.

(A) Synthesis of $[M^{II}(bpy)_3][M^{II}_2(ox)_3]$. M^{II} for the cation can in principle be varied and we verified it for Fe^{II}, Co^{II}, and Ni^{II}. The same holds for M^{II} with respect to the oxalate-bridged network, and examples for Mn^{II}, Fe^{II} are presented in detail. The following synthetic procedure is representative. To a 0.01 M aqueous solution of a $[M^{II}(bpy)_3]^{2+}$ salt, a stoichiometric quantity of a M^{II} salt was added with stirring at room temperature. To the clear solution, a stoichiometric quantity of a 0.02 M aqueous solution of oxalic acid, or alternatively of ammonium oxalate, was added slowly in a second step. A microcrystalline precipitate started to appear after a few minutes; it was filtered off, washed with water, and dried in air.

$[Fe^{II}(bpy)_3][Fe^{II}_2(ox)_3]$ (1). This compound was prepared as red microcrystals. The X-ray powder diffraction data showed it to be structurally isomorphous to the single crystals of compound **3** and to the stoichiometrically identical single crystals prepared by a previously described photochemical pathway.[20] The Mössbauer data are consistent with the stoichiometry (see Results and Discussion). Anal. Calcd for $C_{36}H_{24}N_6O_{12}Fe_3$: C, 48.03; H, 2.69; N, 9.34; Fe, 18.61. Found: C, 47.89; H, 2.94; N, 9.08; Fe, 17.38.

$[Fe^{II}(bpy)_3][Mn^{II}_2(ox)_3]$ (2). This compound was prepared as red microcrystals. The X-ray powder diffraction data showed it to be structurally isomorphous to the single crystals of compound **3**. The Mössbauer data are nearly consistent with the stoichiometric formula. Up to 5% Fe^{II} has been incorporated into the Mn^{II} oxalate-bridged network (see Results and Discussion). Anal. Calcd for $C_{36}H_{24}N_6O_{12}Mn_2Fe$: C, 48.13; H, 2.69; N, 9.35; Mn, 12.23; Fe, 6.22. Found: C, 48.29; H, 2.91; N, 9.08; Mn, 11.69; Fe, 6.12.

Single-Crystal Growth. For growing single crystals,[23] typically a sodium metasilica gel containing 0.01 M oxalic acid was allowed to set in a test tube. Then, stoichiometric quantities of a 0.01 M aqueous solution of the $[M^{II}(bpy)_3]^{2+}$ salt and the additional M^{II} salt for the oxalate-bridged network were added. Within several days, octahedral shaped single crystals formed within the gel.

$[Ni^{II}(bpy)_3][Mn^{II}_2(ox)_3]$ (3). Single crystals were grown with the gel technique and an X-ray structural analysis was completed. Anal. Calcd for $C_{36}H_{24}N_6O_{12}Mn_2Ni$: C, 47.98; H, 2.68; N, 9.33; Mn, 12.19; Ni, 6.51. Found: C, 46.93; H, 2.76; N, 9.55; Mn, 11.70; Ni, 6.59.

$[Fe^{II}(bpy)_3][Co^{II}_2(ox)_3]$, $[Ni^{II}(bpy)_3][Zn^{II}_2(ox)_3]$, and $[Co^{II}(bpy)_3][Mn^{II}_2(ox)_3]$. These compounds, prepared as microcrystalline precipitates, demonstrate the chemical versatility of these 3D systems. They form a structurally isomorphous series, as confirmed by X-ray powder diffraction data. Anal. Calcd for $C_{36}H_{24}N_6O_{12}FeCo_2$: C, 47.71; H, 2.67; N, 9.27; Fe, 6.16; Co, 13.01. Found: C, 47.13; H, 2.74; N, 9.07; Fe, 6.19; Co, 12.95. Anal. Cacld for $C_{36}H_{24}N_6O_{12}NiZn_2$: C, 46.89; H, 2.62; N, 9.11; Ni, 6.37; Zn, 14.18. Found: C, 44.69; H, 2.62; N, 8.69; Ni, 6.36; Zn, 14.24. Anal. Calcd for $C_{36}H_{24}N_6O_{12}Mn_2Co$: C, 47.97; H, 2.68; N, 9.32; Mn, 12.19; Co, 6.54. Found: C, 45.84; H, 2.74; N, 8.99; Mn, 11.89; Co, 6.53.

(B) Synthesis of $[M^{II}(bpy)_3][M^{I}M^{III}(ox)_3]$. In the case of these bimetallic networks we verified the synthetic approach for M^{I} (Li^+, Na^+) and for M^{III} (Cr^{III}, Fe^{III}). No positive results could be seen with M^{I} chosen from K^+ to Cs^+. The synthetic procedure for a general metal combination is representative. To a 0.01 M aqueous solution of a $K_3[M^{III}(ox)_3]\cdot 3H_2O$ complex salt was added a stoichiometric quantity of an aqueous 0.01 M solution of a $[M^{II}(bpy)_3]^{2+}$ salt with stirring at room temperature. After further addition of a stoichiometric amount of a 0.02 M aqueous solution of a M^{I} salt (chloride or nitrate), an immediate microcrystalline precipitation occurred. It was filtered off, washed with water, and dried in air. The X-ray powder diffraction data showed the compounds to be structurally isomorphous, showing only a characteristic line shift from the Li^+ to the Na^+ compounds.

$[Fe^{II}(bpy)_3][LiFe^{III}(ox)_3]$ and $[Fe^{II}(bpy)_3][NaCr^{III}(ox)_3]$. Microcrystalline precipitates were prepared. Anal. Calcd for $C_{36}H_{24}N_6O_{12}LiFe_2$: C, 50.80; H, 2.84; N, 9.87; Li, 0.82; Fe, 13.12. Found: C, 50.67; H, 3.00; N, 10.06; Li, 0.69; Fe, 12.45. Anal. Calcd for $C_{36}H_{24}N_6O_{12}NaCrFe$: C, 50.08; H, 2.80; N, 9.73; Na, 2.66; Cr, 6.02; Fe, 6.47. Found: C, 50.10; H, 2.93; N, 10.00; Na, 2.60; Cr, 6.06; Fe, 6.46.

Single-Crystal Growth. For the single-crystal growth, typically a tetramethoxysilane gel containing a 0.005 M $K_3[M^{III}(ox)_3]\cdot 3H_2O$ salt was allowed to set in a test tube. Then, the test tube was filled with stoichiometric quantities of a 0.01 M aqueous solution of the $[M^{II}(bpy)_3]^{2+}$ salt and the additional M^{I} salt for the oxalate-bridged network. Within several days, tetrahedral shaped single crystals were formed in the gel.

$[Fe^{II}(bpy)_3][NaFe^{III}(ox)_3]$ (4) and $[Fe^{II}(bpy)_3][LiCr^{III}(ox)_3]$ (5). Single crystals were grown with the gel technique and an X-ray structural analysis was performed. Anal. Calcd for $C_{36}H_{24}N_6O_{12}NaFe_2$ (**4**): C, 49.86; H, 2.79; N, 9.69; Na, 2.65; Fe, 12.88. Found: C, 49.79; H, 3.00; N, 9.72; Na, 2.55; Fe, 12.52. Anal. Calcd for $C_{36}H_{24}N_6O_{12}LiCrFe$ (**5**): C, 51.03; H, 2.85; N, 9.92; Li, 0.82; Cr, 6.14; Fe, 6.59. Found: C, 50.74; H, 2.77; N, 10.16; Li, 0.72; Cr, 6.19; Fe, 6.54.

X-ray Crystallographic Analysis. Relevant crystallographic data and structure determination parameters for the three cubic 3D structures of compounds **3**, **4**, and **5** are given in Table 1. Compound **3** was directly related to the known structure of the analogous, but photochemically synthesized iron(II) compound.[20] The observed systematic absences $h00$ with $h \neq 4n$ were in accordance with the possible space groups $P4_332$ or $P4_132$. The refinement was started in space group $P4_332$ (No. 212) with coordinates, including H-atoms, taken from the above-cited iron(II) compound. However, as indicated by SHELXL-93,[27] the enantiomorphic space group $P4_132$ (No. 213) appeared to be more appropriate for the crystal under investigation. In the final refinement, merohedric twinning was observed; twin ratios are given in the footnote of Table 1. The structures of **4** and **5** were solved by direct methods using SHELXS-86.[24]

(20) Decurtins, S.; Schmalle, H. W.; Schneuwly, P.; Oswald, H. R. *Inorg. Chem.* **1993**, *32*, 1888.
(21) Palmer, R. A.; Piper, T. S. *Inorg. Chem.* **1966**, *5*, 864.
(22) Bailar, J. C.; Jones, E. M. In *Inorganic Synthesis*; Booth, H. S., Ed.; McGraw-Hill: New York, 1939; Vol. 1, p 35.
(23) Henisch, H. K. *Crystal Growth in Gels*; Pennsylvania State University: University Park, PA, 1973.
(24) Sheldrick, G. M. *Acta Crystallogr.* **1990**, *A46*, 467.

Table 1. Crystal Data and Structure Determination Parameters[a]

	$[Ni^{II}(bpy)_3]^{2+}{}_n[Mn^{II}_2(ox)_3]_n^{2n-}$ (3)	$[Fe^{II}(bpy)_3]^{2+}{}_n[NaFe^{III}(ox)_3]_n^{2n-}$ (4)	$[Fe^{II}(bpy)_3]^{2+}{}_n[LiCr^{III}(ox)_3]_n^{2n-}$ (5)
formula	$C_{36}H_{24}N_6O_{12}Mn_2Ni$	$C_{36}H_{24}N_6O_{12}NaFe_2$	$C_{36}H_{24}N_6O_{12}LiCrFe$
fw	901.20	867.30	847.40
T, K	293(2)	293(2)	293(2)
radiation	graphite monochromatized, Mo Kα (λ = 0.71073 Å)		
crystal system	cubic	cubic	cubic
space group	$P4_132$ (No. 213)[h]	$P2_13$ (No. 198)	$P2_13$ (No. 198)
a, Å	15.579(2)	15.507(3)	15.262(4)
V, Å^3	3781.1(8)	3728.9(12)	3555(2)
Z	4	4	4
calcd density, g cm^{-3}	1.583	1.545	1.583
obsd density, g cm^{-3}	1.58	1.55	1.60
μ, cm^{-1}	12.22	8.62	7.89
transmission factor[b] range	0.6518–0.6869	0.7155–0.8169	0.7698–0.8311
$F(000)$	1824	1764	1724
crystal size, mm	0.40 × 0.40 × 0.40	0.35 × 0.35 × 0.20	0.29 × 0.29 × 0.29
2θ range (deg)	3.7–69.86	3.7–71.94	3.7–71.86
scan speed (deg/min)	1.5–16.5	1.5–5.5	1.37–5.5
index range, h,k,l	−14/25, −14/25, −14/25	−14/25, −14/25, −14/25	0/25, 0/25, 0/25
reflns measured	11225	11761	9175
unique reflcns	2790	3705	3056
R_{int}	0.027	0.034	0.030
refinement method	full-matrix least-squares on F^2 for all three compounds		
reflcns used	2790	3705	3056
parameters	106	205	205
goodness-of-fit on F^2	1.070	1.045	0.971
final R_1[c] and wR_2[d] indices based on F and F^2, $I > 2\sigma(I)$	0.0341, 0.0738	0.0386, 0.0769	0.0403, 0.0840
R_1 and wR_2 indices (all data)	0.1381, 0.1104	0.1075, 0.0960	0.1176, 0.1120
weight multiplier n[e]	0.0319	0.0231	0.0384
absolute structure parameter[f]	0.42(3)	−0.02(2)	−0.06(3)
2nd extinction[g] parameter	0.0014(2)	0.0089(4)	0.0005(2)
max shift/esd	0.046	0.002	0.002
min, max peaks (e/Å^3)	−0.309, 0.632	−0.297, 0.483	−0.393, 0.798

[a] Data for all three compounds were collected on an Enraf-Nonius CAD-4 diffractometer. Unit cell parameters were obtained from the least-squares refinement of the θ angles of 25 reflections with 19.0° < 2θ < 24.0° for **3**, 19.3° < 2θ < 37.0° for **4**, and 16.2° < 2θ < 43.6° for **5**. [b] Absorption corrections based on eight (**3**), five (**4**), and four (**5**) indexed and measured crystal faces. Tetrahedra forms for **4** and **5** found by indexing the crystal faces are {111}. A counterface of (−1−11) was observed for the measured crystal of **4**. [c] R_1 factor definition: $R_1 = \sum(||F_o|-|F_c||)/\sum|F_o|$. [d] SHELXL-93 wR_2 factor definition: $wR_2 = [\sum w(F_o^2 - F_c^2)^2/\sum w(F_o^2)^2]^{1/2}$. [e] Weighting scheme: $w = 1/[\sigma^2(F_o)^2 + (np)^2 + 0.00p]$, $p = (\max(F_o^2) + 2F_c^2)/3$. [f] Expected values for the absolute structure parameter are 0 (within 3 esd's) for correct and +1 for inverted absolute structure. [g] The secondary extinction parameter x was refined by least squares, where F_o is multiplied by $-^1/_4k[1 + 0.001xF_c^2\lambda^3/\sin(2\theta)]$. [h] According to merohedric twinning the space groups are $P4_332$ (no. 212) for twin I (42%) and $P4_132$ (no. 213) for twin II (58%).

The systematic absences were consistent with the $P4_232$ and $P2_13$ space groups. Within the cubic system, $P2_13$ is a non-isomorphic subgroup of both $P4_332$ and $P4_132$, while $P4_232$ is not. The successful structure determination of **4** clearly showed the space group $P2_13$ as being correct. For compound **4**, two missing carbon atoms of the bpy ligand were finally found in the difference electron density map. All non-hydrogen atoms were refined anisotropically; H-atom positions from difference maps were refined isotropically. Since compound **5** was likely to be isostructural with **4**, the atomic coordinates of **4** were used as a starting point, only replacing Na by Li and Fe by Cr. Data collection, unit cell refinement, and crystal face indexing were carried out with the Enraf-Nonius CAD-4 software.[25] Three (two) standard reflections were measured every 3 h for **3**, **4**, and **5**. No significant decrease in intensities was noted for any of the three crystals. To control orientation, three reflections were checked every 400 reflections during each data collection. Intensity data were corrected for Lorentz, polarization, and absorption effects using the MolEN[26] program system. Refinements on F_o^2 using all unique reflections were carried out with SHELXL-93,[27] which is also an excellent tool for absolute structure determination, using Flack's x-parameter refinement.[28] Friedel pairs ($\bar{h},\bar{k},\bar{l}$) were measured for **3** and **4** in the range 1° < θ < 20°. As **5** was suspected to be isostructural with **4**, only the positive hkl data were collected. Test calculations with and without Friedel pairs resulted in the same chirality (Λ-configuration) for **4** and **5**. The corresponding x-parameters and their esd's differed only minimally within the range of 1σ for **3**: x = 0.44(3) without and 0.42(3) with Friedel pairs. The values for compound **4** are x = 0.04(3) without and −0.02(2) with Friedel pairs. Significant differences in bond lengths and angles could not be observed.

Absolute Structure Determination. The merohedral crystal structures presented here belong to the chiral crystal classes, therefore a separate discussion will be given to some relevant aspects of this matter. An ambiguity table for the non-centrosymmetric crystal classes is given by Jones.[29] The ambiguities in merohedral crystal classes are discussed from the group-theoretical point of view by Burzlaff and Hümmer.[30] In a review[31] concerning the enantiomorph-polarity estimation by means of Flack's x-parameter refinement, practical experiences with 15 "absolute-structure" (Jones[32]) determinations are illustrated. The absolute structure parameter (see Table 1) or Flack's x-parameter refinement (Flack;[33] Bernardinelli and Flack[28]) is an important tool for the determination of possibly merohedrically twinned crystal structures. Early work on twinning by merohedry and the occurrence of two classes of twins by merohedry in the 32 crystal point groups are demonstrated by Catti and Ferraris.[34] Systematic definitions of possible twins with examples for several space groups and also the consideration of twinning by merohedry are discussed by Koch.[35] The theoretical and historical background of absolute structure determination using the X-ray dispersion corrections in crystal structure refinements is summarized in a review given by Creagh and McAuley.[36]

Glazer and Stadnicka[37] recommended an extension of the term "absolute" in the concept of "absolute structure" as introduced by Jones:

(25) Enraf-Nonius CAD-4 Software, Version 5.0, Enraf-Nonius, Delft, The Netherlands, 1989.
(26) Fair, C. K., MolEN. An interactive intelligent system for crystal structure analysis, Enraf-Nonius, Delft, The Netherlands, 1990.
(27) Sheldrick, G. M. *J. Appl. Crystallogr.*, in preparation.
(28) Bernardinelli, G.; Flack, H. D. *Acta Crystallogr.* **1985**, *A41*, 500.
(29) Jones, P. G. *Acta Crystallogr.* **1986**, *A42*, 57.
(30) Burzlaff, H.; Hümmer, K. *Acta Crystallogr.* **1988**, *A44*, 506.
(31) Müller, G. *Acta Crystallogr* **1988**, *B44*, 315.
(32) Jones, P. G. *Acta Crystallogr.* **1984**, *A40*, 660.
(33) Flack, H. D. *Acta Crystallogr.* **1983**, *A39*, 876.
(34) Catti, M.; Ferraris, G. *Acta Crystallogr.* **1976**, *A32*, 163.
(35) Koch, E. In *International Tables for Crystallography*; Wilson, A. J. C., Ed.; Kluwer Academic Publishers: Dordrecht, Boston, London, 1992; Vol. C, pp 10–14.
(36) Creagh, D. C.; McAuley, W. J. In *International Tables for Crystallography*; Wilson, A. J. C., Ed.; Kluwer Academic Publishers: Dordrecht, Boston, London, 1992, Vol. C, pp 206–222.
(37) Glazer, A. M.; Stadnicka, K. *Acta Crystallogr.* **1989**, *A45*, 234.

[32] the structure has to be related to some macroscopic physical properties, e.g. when the "absolute structure" is linked to the crystal habit, the proposed term is *absolute morphology*; for the enantiomorphic merohedries (11 crystal classes) it is *absolute chirality* (which is linked e.g. with optical activity). Such an example of absolute structure determination in this sense was presented recently by Stadnicka, Glazer, and Arzt[38] in their discussion of the structure of $KLiSO_4$. Considering the improvement in the reliability of the absolute structure determination by refining crystal structures on F_o^2, the structure of the recently reported iron(II) compound[20] (identical to **1**) has been recalculated with the new program SHELXL-93, refining Flack's x-parameter to $x = 0.0100$ with an esd of 0.0323, which confirms the reported absolute structure in space group $P4_332$. By chance, the structure of the chosen crystal of **3** appeared to be merohedrically twinned (see Table 1), with twin ratios of 42/58 (esd 3%).

Before introducing Flack's x-parameter refinement, it was common practice to determine the absolute configuration of non-centrosymmetric structures with the aid of Hamilton's[39] R-factor ratio test. Critical comments about this practice were stated by Rogers,[40] who proposed the alternative η-parameter refinement as a means and improvement of absolute configuration determination. This was successfully confirmed by G. M. Sheldrick, who implemented the η-parameter in his program SHELXTL for the Eclipse computer at that time. However, both the Hamilton R-factor ratio test and the η-parameter refinement are inconclusive for merohedral twins. In general cases one does not know if a twin is present or not, and even if the presence of twinning by merohedry is known, the twin ratio is still unknown. Flack[33] solved this problem by treating every non-centrosymmetric crystal as an inversion (or merohedral) twin when he introduced the refinement of x (which is the fraction of one of the twins). This procedure was thoroughly worked out by Bernardinelli and Flack[28] and checked with respect to the effects of absorption correction, data region, stability constant, and neglect of light atoms.[41] Hence, Flack's x-parameter refinement is now commonly well accepted and implemented e.g. in the program systems XTAL,[42] CRYSTALS,[43] and SHELXL-93;[27] and it clearly differentiates between possible chirality/polarity and determines the corresponding ratios of the configurations.

As compounds **4** and **5** crystallize in space group $P2_13$ with nicely grown tetrahedral morphology, forms {111} or $\{\bar{1}\bar{1}\bar{1}\}$ can easily be distinguished with the Enraf-Nonius CAD-4 software.[25] This information was also used for numerical absorption corrections before the data sets were merged. According to Glazer and Stadnicka,[37] the absolute morphology of **4** and **5** could be determined, since their absolute structures (Λ-configuration for both) are linked to the crystal form {111}.

To summarize, for both types of networks, the crystal structures with the Δ-configuration crystallize either in space group $P4_332$ (No. 212) or in space group $P2_13$ with the tetrahedral form $\{\bar{1}\bar{1}\bar{1}\}$. The Λ-configuration corresponds with the tetrahedral form {111} or, in the higher symmetry, with the space group $P4_132$ (No. 213).

Mössbauer Spectroscopy. A constant-acceleration type Mössbauer spectrometer together with a 1024-channel analyzer operating in the time scale mode was employed. The source, $^{57}Co/Rh$ (25 mCi, Amersham Buchler), was kept at room temperature for all measurements. The velocity calibration was performed with the known hyperfine splittings in the spectrum of metallic iron and the isomer shifts reported here are relative to α-Fe at room temperature. Spectra of the samples were collected between 293 and 4.2 K by means of a He continuous flow cryostat (Model CF500, Oxford Instruments).

Magnetic Measurements. These measurements were performed in the temperature range 2.0–300 K with a vibrating-sample magnetometer (Foner magnetometer, Princeton Applied Research) equipped with a combined He-bath-continous-flow cryostat built by Cryovac (Troisdorf, Germany). Tetrakis(thiocyanato)mercury cobaltate was used as a susceptibility standard. The magnetic susceptibility data were obtained on powdered samples of about 35 mg in a field of 1 T. The presence of ferromagnetic impurities could be excluded by field-dependent measurements. All the observed susceptibilities were corrected for the diamagnetism estimated from Pascal's tables {-429×10^{-6} cm^3 mol^{-1} for **1**, -431×10^{-6} cm^3 mol^{-1} for **2**, -413×10^{-6} cm^3 mol^{-1} for $[Fe^{II}(bpy)_3][LiFe^{III}(ox)_3]$}, and the temperature independent paramagnetism (TIP) was taken to be 200×10^{-6} cm^3 mol^{-1} for all complexes.[44]

Table 2. Selected Bond Lengths (Å) and Angles (deg) for **3**

		Distances	
Ni–N1	2.088(2) 6×	C3–C4	1.374(5)
		C4–C5	1.378(5)
Mn–O21	2.154(2) 3×	C5–C6	1.395(4)
Mn–O11	2.166(2) 3×	C6–C6a	1.484(5)
		O11–C11	1.236(2) 2×
N1–C2	1.326(3)	O21–C21	1.241(2) 2×
N1–C6	1.350(3)	C11–C21	1.577(5)
C2–C3	1.381(4)		
		Angles	
N1–Ni–N1	92.4(1) 3×	O11–Mn–O11	90.0(1) 3×
N1–Ni–N1	79.0(1) 3×	O11–Mn–O21	93.7(1) 3×
N1–Ni–N1	94.7(1) 6×	O11–Mn–O21	167.0(1) 3×
N1–Ni–N1	170.8(1) 3×	O21–Mn–O21	99.2(1) 3×
C2–N1–Ni	126.0(2)	O11–Mn–O21	77.6(1) 3×
C6–N1–Ni	114.8(2)	C11–O11–Mn	113.8(2)
		C21–O21–Mn	113.9(2)
C2–N1–C6	119.1(2)	C5–C6–C6a	123.5(2)
N1–C2–C3	123.1(3)	N1–C6–C6a	115.7(1)
C4–C3–C2	118.0(3)	O11–C11–O11	125.7(3)
C3–C4–C5	119.9(3)	O11–C11–C21	117.2(2) 2×
C4–C5–C6	119.1(3)	O21–C21–O21	126.0(4)
N1–C6–C5	120.8(3)	O21–C21–C11	120.8(3) 2×

Results and Discussion

Description of the Structures. Basically, both types of anionic networks, $[M^{II}_2(ox)_3]_n^{2n-}$ and $[M^{I}M^{III}(ox)_3]_n^{2n-}$, form an analogous three-dimensional pattern, but as they differ in stoichiometry, they must be described in different space groups. For both types, the formal $[M(ox)_{3/2}]$ subunits, representing 3-connecting points, build up well-defined 3D 3-connected 10-gon nets (10,3)[45] with $[M^{II}(bpy)_3]^{2+}$ cations occuping the vacancies in strictly the same manner. Firstly, the results of the $[M^{II}_2(ox)_3]_n^{2n-}$ type structure will be summarized, but for a detailed discussion and the overall representation we refer to an earlier report.[20] In a complementary way we intend to concentrate on the illustration and characteristics of the $[M^{I}M^{III}(ox)_3]_n^{2n-}$ type nets.

(A) Compound **3** was chosen for a representative structural analysis of the 3D $[M^{II}_2(ox)_3]^{2-}$ type network prepared by the gel technique and, as a first consideration, the aim was to prove that **3** was structurally identical to the photochemically synthesized $[Fe^{II}(bpy)_3][Fe^{II}_2(ox)_3]$ single crystals.[20] Apart from the chirality, the structural identity of **3** to the earlier reported iron(II) compound is clearly established. Table 2 specifies selected bond lengths and angles, whereby the atomic numbering can be related to Figure 1. The larger Mn–O distance of 2.160 Å, compared with the mean value of 2.125 Å for Fe–O in the case of the analogous iron(II) net, brings about a larger lattice parameter and an increase of the cell volume of 3.7%. Looking at the geometry of the manganese coordination, the trigonally distorted octahedral MnO_6 unit may be represented by a simple model which is described by the degree of compression and by an angle of twisting.[46] An octahedron, viewed along a C_3 axis, exhibits two perfectly staggered equilateral triangles of side s, which are exactly $h = (2/3)^{1/2}$ s apart. The ratio s/h determines the compression factor (1.22 for the regular octahedron) and ϕ the twisting of the triangles with respect to each other (60° for the regular octahedron). The tris(oxalato)–manganese complex reveals an angle ϕ of 48° (identical to ϕ for the iron(II) complex) and a s/h ratio of 1.39 (s = 3.168 Å (mean value), h = 2.281 Å), compared with 1.42 for the iron(II) complex. However, one has to take account of the fact that these results are based on an

(38) Stadnicka, K.; Glazer, A. M.; Arzt, S. *J. Appl. Crystallogr.* **1993**, *26*, 555.
(39) Hamilton, W. C. *Acta Crystallogr.* **1965**, *18*, 502.
(40) Rogers, D. *Acta Crystallogr.* **1981**, *A37*, 734.
(41) Bernardinelli, G.; Flack, H. D. *Acta Crystallogr.* **1987**, *A43*, 75.
(42) Stewart, J. M.; Hall, S. R., Eds. *The XTAL System of Crystallographic Programs*—User's Manual; University of Maryland: College Park, Maryland, 1990.
(43) Carruthers, J. R.; Watkin, D. L. *Crystals*; Chemical Crystallography Laboratory: Oxford, England, 1986; Issue 9.
(44) Casey, T. In *Theory and Application of Molecular Paramagnetism*; Boudreaux, E. A., Mulay, L. N., Eds.; John Wiley & Sons: New York, 1976; Chapter 2.
(45) Wells, A. F. *Structural Inorganic Chemistry*; Clarendon Press: Oxford, England, 1984.
(46) Stiefel, E. I.; Brown, G. F. *Inorg. Chem.* **1972**, *11*, 434.

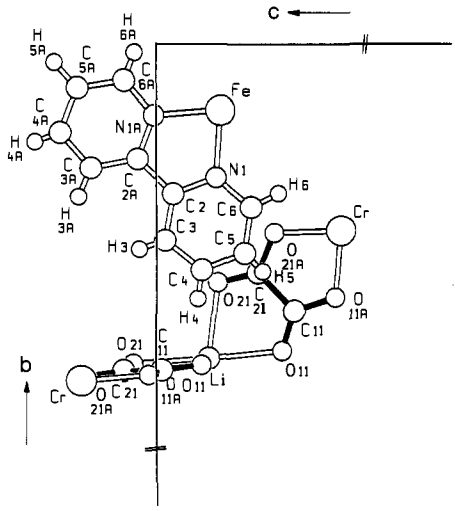

Figure 1. Sector from a [100] projection, showing the asymmetric unit in the $[M^{II}(bpy)_3][M^{I}M^{III}(ox)_3]$ type network and the molecular arrangement between bpy and oxalate ligands.

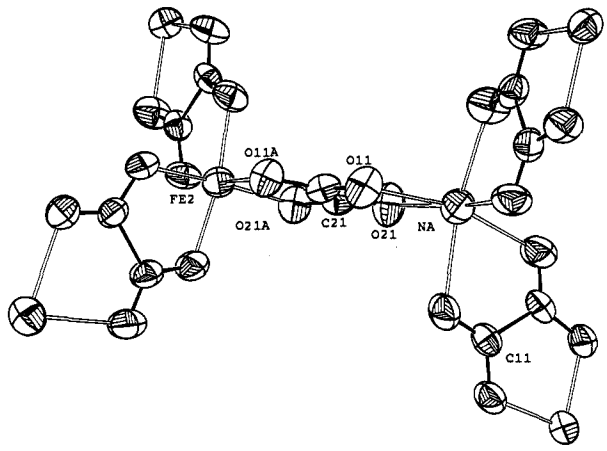

Figure 2. ORTEP plot (50% probability level) of Na and Fe2 coordination in the three-dimensional oxalate-bridged network **4**.

assumption of regular distortion, and an inspection of the relevant bond angles (O11–M–O11 and O21–M–O21) shows clearly some deviation from regularity.

(**B**) For the structure determination of the 3D $[M^{I}M^{III}(ox)_3]^{2-}$ type network, compounds **4** and **5** were selected. According to the lower symmetry compared with $P4_132/P4_332$ (the 2-fold axis is missing in $P2_13$), the asymmetric unit contains a complete oxalate ligand, both metals of the network and the complete bpy ligand. Figure 1, a [100] projection of this asymmetric unit, shows the atomic numbering and in addition the mutual arrangement of the bpy and oxalate ligands. Figures 2 and 3 display the thermal ellipsoid plots of the metal coordination within the networks of **4** and **5**. The planar oxalate ligands repeatedly bridge the metal ions in all three dimensions, and in both of the measured crystals, the tris-chelating subunits were found to be in the Λ-configuration.

Selected bond lengths and angles are given in Table 3. Notable is the pronounced asymmetry in the Li coordination with two different sets of Li–O bond lengths. An analogous asymmetry was recently reported in the case of a similar LiO_6 coordination.[47]

Figure 4[48] shows a [100] projection of the $[LiCr^{III}(ox)_3]_n^{2n-}$ net and the true analogy to the M^{II}_2-type network is obvious. Only the existence of two different metal ions reduces a 4-fold symmetry axis (4_1 or 4_3 screw axis) to a 2_1-axis, hence the change

(47) Declercq, J. P.; Feneau-Dupont, J.; Ladriere, J. *Polyhedron* **1993**, *12*, 1031.

(48) SCHAKAL86, a Fortran program for the graphic representation of molecular and crystallographic models: Keller, E. *Chem. Unserer Zeit* **1986**, *20*, 178.

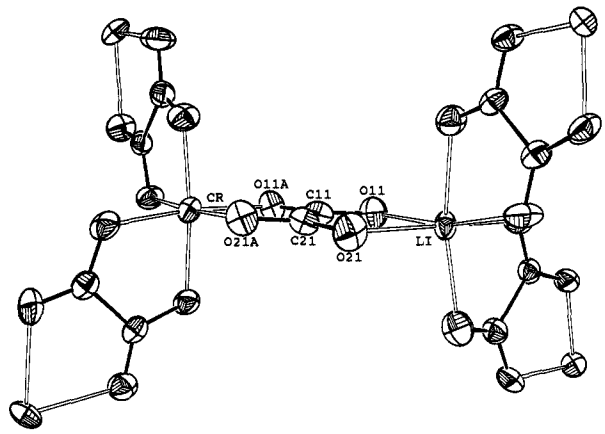

Figure 3. ORTEP plot (50% probability level) of Li and Cr coordination in the three-dimensional oxalate-bridged network **5**.

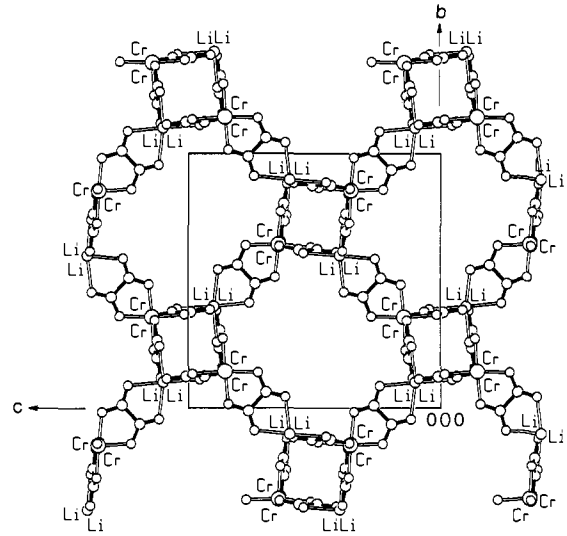

Figure 4. [100] projection of $[LiCr(ox)_3]_n^{2n-}$ for compound **5**.[48]

from space groups $P4_332/P4_132$ to $P2_13$. Figure 5, an alternative stereoview, emphasizes the 2-fold screw axis by exhibiting one of the helical strands, which all together form the 3D network. The Λ-configuration of the chiral $[M(ox)_{3/2}]$ subunits produces right-handed helical strands. Correspondingly, subunits with a Δ-configuration will bring about a left-handed helicity. Both metal ions within the network occupy sites with symmetry 3 (Wyckoff letter a), as in the case of the M^{II}_2-type network. Figure 6, a stereoplot of the anionic network, gives a detailed insight into the 3-connected 10-gon (10,3) net and demonstrates also that the topology is analogous to the M^{II}_2-type net.

The tris-chelating $[M^{II}(bpy)_3]^{2+}$ cations occupy the vacancies in the same manner as was previously described for the M^{II}_2-type nets, only that the site symmetry for the central metal ion is now lowered from 32 to 3 (Wyckoff letter a). With respect to the chirality, the cations are found to be in the Λ-configuration for both compounds **4** and **5**, which again demonstrates the preference for the Λ–Λ or Δ–Δ combination between the configurations of the cations and the anionic nets.

An examination of the relative geometric positions of the planar bpy and oxalate ligands, as depicted in Figure 1, shows no particular kind of stacking, although the planes are nearly coplanar (tilt angle 8.9°). Apparently, for geometrical reasons, the contacts are not fully at the limit of van der Waals radii; the distance between O21A or O21 and the bpy plane is 3.59 or 3.96 Å, respectively.

Mössbauer Spectroscopy. The synthetic approach for the $[M^{II}(bpy)_3][M^{II}_2(ox)_3]$ type compounds presented earlier needs some additional comments. When different M^{II} ions are used for the cations and the anionic net, the stoichiometric formula has to be

Table 3. Selected Bond Lengths (Å) and Angles (deg) for **4** and **5**

4		5	
	Distances		
Fe1–N1	1.977(2) 3×	Fe–N1	1.972(3) 3×
Fe1–N1a	1.977(2) 3×	Fe–N1a	1.971(2) 3×
Fe2–O11a	2.002(2) 3×	Cr–O11a	1.980(2) 3×
Fe2–O21a	1.986(2) 3×	Cr–O21a	1.975(2) 3×
Na–O11	2.320(3) 3×	Li–O11	2.164(8) 3×
Na–O21	2.317(3) 3×	Li–O21	2.243(7) 3×
N1–C6	1.339(4)	N1–C6	1.345(4)
N1–C2	1.357(4)	N1–C2	1.352(4)
C2–C3	1.386(4)	C2–C3	1.395(5)
C2–C2a	1.475(4)	C2–C2a	1.466(4)
C3–C4	1.390(5)	C3–C4	1.383(6)
C4–C5	1.362(5)	C4–C5	1.352(7)
C5–C6	1.376(5)	C5–C6	1.376(5)
N1a–C6a	1.332(4)	N1a–C6a	1.340(4)
N1a–C2a	1.372(4)	N1a–C2a	1.358(4)
C2a–C3a	1.376(4)	C2a–C3a	1.389(5)
C3a–C4a	1.385(5)	C3a–C4a	1.377(6)
C4a–C5a	1.360(6)	C4a–C5a	1.367(7)
C5a–C6a	1.383(5)	C5a–C6a	1.379(6)
O11–C11	1.214(4)	O11–C11	1.227(4)
O21–C21	1.221(4)	O21–C21	1.224(4)
O11a–C11	1.264(4)	O11a–C11	1.279(4)
O21a–C21	1.269(4)	O21a–C21	1.288(4)
C11–C21	1.582(4)	C11–C21	1.550(5)
	Angles		
N1a–Fe1–N1a	93.9(1) 3×	N1a–Fe–N1a	94.1(1) 3×
N1a–Fe1–N1	90.6(1) 3×	N1a–Fe–N1	90.2(1) 3×
N1a–Fe1–N1	81.8(1) 3×	N1a–Fe–N1	81.9(1) 3×
N1a–Fe1–N1	174.0(1) 3×	N1a–Fe–N1	174.4(1) 3×
N1–Fe1–N1	94.0(1) 3×	N1–Fe–N1	94.0(1) 3×
C6–N1–Fe1	126.7(2)	C6–N1–Fe	126.5(3)
C2–N1–Fe1	115.0(2)	C2–N1–Fe	114.5(2)
C6a–N1a–Fe1	127.9(2)	C6a–N1a–Fe	127.0(2)
C2a–N1a–Fe1	115.0(2)	C2a–N1a–Fe	114.8(2)
O21a–Fe2–O21a	93.6(1) 3×	O21a–Cr–O21a	94.4(1) 3×
O11a–Fe2–O21a	95.4(1) 3×	O11a–Cr–O21a	91.9(1) 3×
O11a–Fe2–O21a	82.0(1) 3×	O11a–Cr–O21a	82.7(1) 3×
O11a–Fe2–O21a	170.2(1) 3×	O11a–Cr–O21a	173.2(1) 3×
O11a–Fe2–O11a	89.7(1) 3×	O11a–Cr–O11a	91.3(1) 3×
C11–O11a–Fe2	114.6(2)	C11–O11a–Cr	113.9(2)
C21–O21a–Fe2	114.6(2)	C21–O21a–Cr	114.4(2)
O21–Na–O21	103.0(1) 3×	O21–Li–O21	100.1(4) 3×
O11–Na–O21	75.0(1) 3×	O11–Li–O21	77.4(1) 3×
O11–Na–O21	92.1(1) 3×	O11–Li–O21	91.8(1) 3×
O11–Na–O21	164.8(1) 3×	O11–Li–O21	168.1(3) 3×
O11–Na–O11	90.0(1) 3×	O11–Li–O11	91.1(4) 3×
C11–O11–Na	111.6(2)	C11–O11–Li	112.9(3)
C21–O21–Na	111.6(2)	C21–O21–Li	110.7(2)
C6–N1–C2	118.3(3)	C6–N1–C2	118.9(3)
N1–C2–C3	121.5(3)	N1–C2–C3	120.6(3)
N1–C2–C2a	114.7(2)	N1–C2–C2a	114.8(3)
C3–C2–C2a	123.9(3)	C3–C2–C2a	124.5(3)
C4–C3–C2	119.1(3)	C4–C3–C2	119.2(4)
C5–C4–C3	118.9(3)	C5–C4–C3	119.5(4)
C4–C5–C6	119.7(4)	C4–C5–C6	119.6(4)
N1–C6–C5	122.6(4)	N1–C6–C5	122.1(4)
C6a–N1a–C2a	117.1(3)	C6a–N1a–C2a	118.2(3)
N1a–C2a–C3a	121.7(3)	N1a–C2a–C3a	121.4(3)
N1a–C2a–C2	113.5(2)	N1a–C2a–C2	113.9(3)
C3a–C2a–C2	124.8(3)	C3a–C2a–C2	124.6(3)
C4a–C3a–C2a	119.5(4)	C4a–C3a–C2a	119.2(4)
C5a–C4a–C3a	119.3(3)	C5a–C4a–C3a	119.3(4)
C4a–C5a–C6a	118.7(4)	C4a–C5a–C6a	119.3(4)
N1a–C6a–C5a	123.8(4)	N1a–C6a–C5a	122.5(4)
O11–C11–O11a	125.0(3)	O11–C11–O11a	125.2(3)
O11–C11–C21	121.0(3)	O11–C11–C21	119.8(3)
O11a–C11–C21	114.0(3)	O11a–C11–C21	115.1(3)
O21–C21–O21a	125.7(3)	O21–C21–O21a	127.1(3)
O21–C21–C11	120.3(3)	O21–C21–C11	119.1(3)
O21a–C21–C11	114.0(3)	O21a–C21–C11	113.8(3)

carefully examined for each compound. Ligand exchange reactions, depending on the kind of $[M^{II}(bpy)_3]^{2+}$ complexes, could bring about an incorporation of the M^{II} ion of the cation into the anionic network to some extent. In the case of iron(II) compounds, this can best be followed with Mössbauer experiments.

In Figure 7, the Mössbauer spectra of compounds **1** and **2** at 10 K are shown. In the case of compound **1**, the spectrum consists of two quadrupole doublets, one being typical for the cationic low-spin Fe(II) complex $[Fe(bpy)_3]^{2+}$ (δ = 0.35 mm s^{-1}, ΔE_Q = 0.40 mm s^{-1}) and the other one characteristic of the high-spin Fe(II) within the anionic $[Fe_2(ox)_3]_n^{2n-}$ net (δ = 1.29 mm s^{-1}, ΔE_Q = 2.10 mm s^{-1}). The anion-to-cation area ratio in the spectrum turns out to be 2:1, being consistent with the stoichiometry of **1**. It is worthwhile noting that this area ratio is about 1:1 in the room temperature spectrum of this compound, indicating very different Debye–Waller factors for the cationic and anionic Fe(II) complexes. The spectrum of compound **2** exhibits essentially the quadrupole doublet of the $[Fe(bpy)_3]^{2+}$ cation showing that the stoichiometry of the compound is nearly perfect. However, weak high-spin Fe(II) resonances (which represent ≈9% of the spectrum) are present, one of which can be attributed to $[Fe^{II}(ox)_{3/2}]^-$ subunits according to its Mössbauer parameters. A small proportion of the ferrous ions (≈5%) has obviously been incorporated into the Mn(II)–oxalato network during the preparation procedure.

Figure 8 shows the Mössbauer spectra of a polycrystalline sample of $[Fe^{II}(bpy)_3][LiFe^{III}(ox)_3]$ at different temperatures (295, 10, and 4.2 K, respectively). The room temperature spectrum is dominated by the quadrupole doublet of the $[Fe(bpy)_3]^{2+}$ cation; the intensity due to the $[Fe^{III}(ox)_{3/2}]$ subunits of the compound takes only about 15% of the whole spectrum, demonstrating again a large difference in the Debye–Waller factors of the cationic and anionic units. The isomer shift of 0.31 mm s^{-1} and the quadrupole splitting of about 1.10 mm s^{-1} are characteristic for a high-spin Fe^{3+} ion in a noncubic environment. The fit of the spectrum at 10 K yields an area ratio of approximately 1:1 for the cation and anion resonance in agreement with nearly perfect stoichiometry. It is known from a recent study of $Li_4[Fe(ox)_3]Cl{\cdot}9H_2O$[47] that the $[Fe^{III}(ox)_{3/2}]$ subunits of the compound exhibit an asymmetry in the line width of the quadrupole pattern. This results from relaxation effects of paramagnetic ions due to fluctuation rates of the internal field comparable to the Larmor frequency of the nuclear magnetic moment.[49] In the present investigation, no attempt was made to take into account this asymmetry characteristic of the Mössbauer resonance during the fit procedure. Because of the close superposition of the two quadrupole patterns due to anions and cations, a quadrupole doublet of equal intensities and widths of two lines was used for $[Fe^{III}(ox)_{3/2}]$ in order to obtain a reasonable fit. A further complication arises with the onset of an overall broadening of the spectrum, which is more pronounced in the spectrum at 4.2 K. Reasons for this behavior could be (i) relaxation effects on the molecular basis due to spin–spin interactions or (ii) the onset of cooperative magnetic ordering in the oxalate-bridged network of the compound. The low temperature (T < 4.2 K) and the external magnetic field dependence of the Mössbauer spectra will be subjects of further investigations.

Magnetic Properties. The thermal variation of the molar magnetic susceptibilities of **1** and **2** is presented in Figure 9. The susceptibility of **2** exhibits a rounded maximum at about 20 K followed by a sharp increase of X_M below 10 K. The maximum in the curve is characteristic of antiferromagnetic coupling in the anionic 3D coordination polymer. This is supported by the value of the Weiss constant θ = −33 K, obtained from a fit of the temperature dependence of X_M^{-1} within the temperature range of 100–300 K to the Curie–Weiss law, which is shown in the same figure. The increase of X_M below 10 K is obviously due to paramagnetic impurities. The effective magnetic moment for **2** at 293 K, calculated by the equation $\mu_{eff} = 2.828(X_M T)^{1/2}$, shows

(49) Blume, M.; Tjon, J. A. *Phys. Rev.* **1968**, *165*, 446.

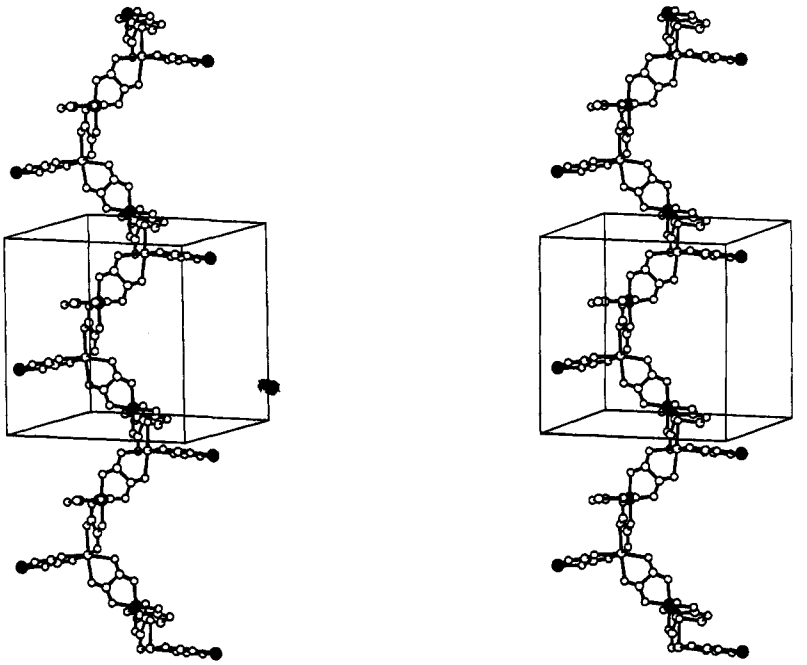

Figure 5. Selected stereoview of the 3D (10,3) network (**4**, **5**) accentuating one of its helical strands along a 2_1 axis (●, M^{III} = Fe or Cr).

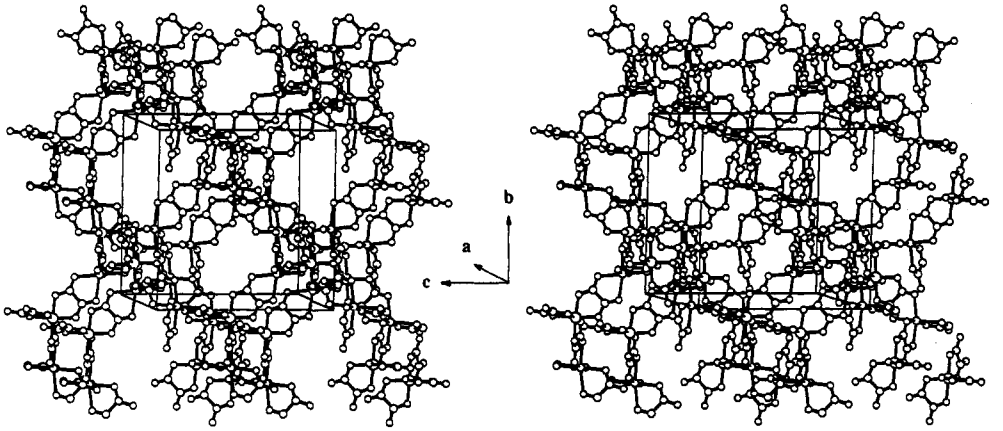

Figure 6. Stereoview of a section of the three-dimensional $[M^{I}M^{III}(ox)_3]$ type network (**4**, **5**).

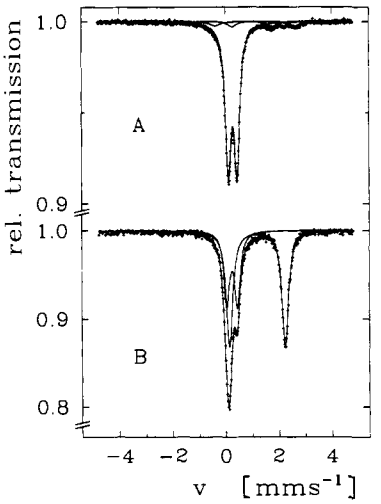

Figure 7. Mössbauer spectra of compounds **2** (A) and **1** (B) at 10 K.

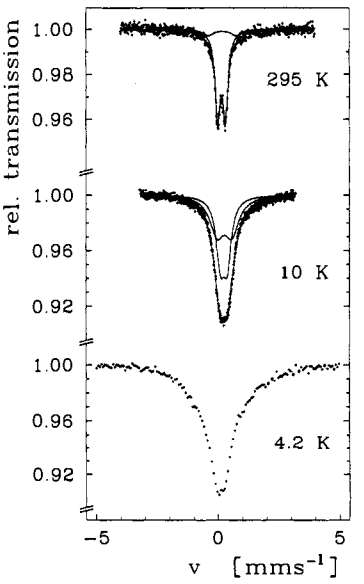

Figure 8. Mössbauer spectra of $[Fe^{II}(bpy)_3][LiFe^{III}(ox)_3]$ recorded at different temperatures.

a value of 5.68 μ_B, which is slightly lower than the spin-only value of 5.9 μ_B for a spin of $^5/_2$. Compound **1** essentially exhibits the same behavior, except that the maximum at around 20 K is more or less obscured by the magnetic contribution of the paramagnetic impurity. The Weiss constant θ turns out to be −28 K. The effective magnetic moment for **1** at 295 K with μ_{eff} = 5.16 μ_B lies slightly above the spin-only value of 4.9 μ_B for a spin of 2.

At this stage of the experiments, no definitive conclusions can be drawn from the magnetic behavior of these polymeric 3D compounds. Therefore, extended, comparative studies are

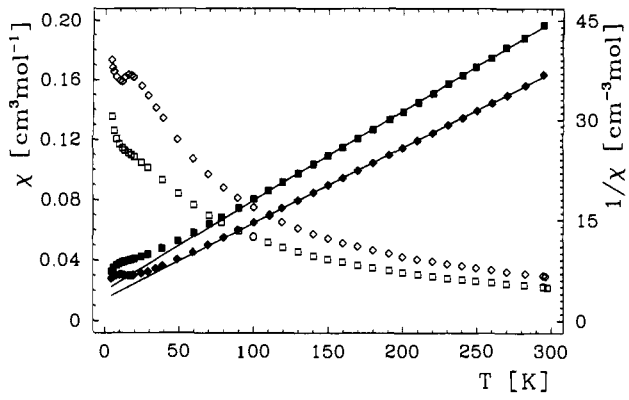

Figure 9. Temperature dependence of the molar magnetic susceptibility χ_M (◇, □) and the inverse susceptibility $1/\chi_M$ (◆, ■) of **1** (□, ■) and **2** (◇, ◆).

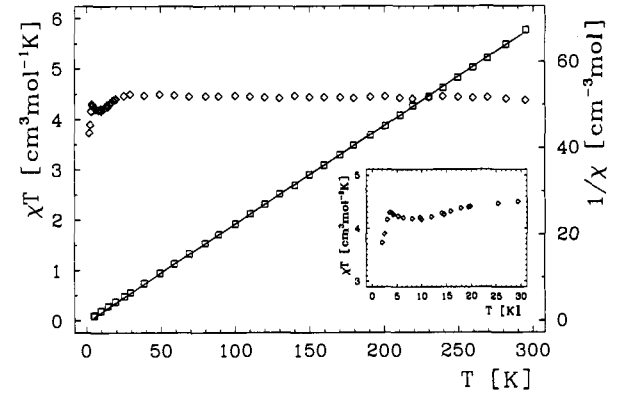

Figure 10. Thermal variation of $\chi_M T$ (◇) and of the inverse susceptibility $1/\chi_M$ (□) per LiFe of $[Fe^{II}(bpy)_3][LiFe^{III}(ox)_3]$. The inset shows the X_MT behavior at low temperatures.

required, which include chemically different systems (M^{II} = Co^{II}, Ni^{II}, Cu^{II}) and, especially, ordered $[M^{II}M^{III}(ox)_3]^-$ type networks, which should also be realizable (see below). It will be of interest to find out how the well-defined topology of the networks is influencing the magnetic properties of these systems.

In case of the $[M^{I}M^{III}(ox)_3]$ type network, the experimental data for $[Fe^{II}(bpy)_3][LiFe^{III}(ox)_3]$ are shown in Figure 10. The X_MT versus T plot shows the typical behavior of a normal paramagnet in the temprature range 30–300 K. Below 30 K, X_MT slightly decreases and reaches a small maximum at about 3.5 K, followed by a sharp decrease at lower temperatures. The high-temperature range (100–300 K) yields a Curie constant C of 4.39 $cm^3\ mol^{-1}\ K$ which is close to the theoretical value of 4.38 $cm^3\ mol^{-1}\ K$ for high-spin d^5 single ions. The Weiss constant θ is 1.5 K. The deviation with respect to the Curie law in this single ion system may have its origin in the zero-field splitting of the ground state of the Fe^{3+} ion; the other possible source of Curie–Weiss behavior—exchange interaction between magnetic ions—will to a great extend be restricted because of the intervening diamagnetic $[Li(ox)_{3/2}]^{2-}$ subunits in the oxalate-bridged network. The decrease below 3.5 K can either be indicative of an antiferromagnetic 3D ordering in the $[LiFe^{III}(ox)_3]_n^{2n-}$ network, which is also one of the possible explanations of the low-temperature Mössbauer data, or due to the decreasing population of the $M_S = \pm^5/_2, \pm^3/_2$ states of the three Kramers doublets within an axial zero-field splitting of the high-spin Fe^{3+} ion with decreasing temperature. The minimum at about 8 K is not understood. Further investigations are being carried out in order to clarify this phenomenon.

Concluding Remarks

We have previously shown that through a photochemical synthetic approach, a three-dimensional oxalate-bridged iron(II) network can be crystallized.[20] With an alternative, straightforward synthetic method, which is mainly based on the function of the tris-chelated metal–bipyridine cations as ideal counterions, this 3D polymeric structure is now accessible on a far larger and more comprehensive scale. Thereby, a variation in the kind of metal ions for the tris-chelated cations, as well as for the oxalate-bridged networks, is now possible.

Whereas this report has concentrated on two types of networks, further combinations can be envisaged, which will enable us to determine how flexible the synthetic concept is. For $[M^{II}M^{III}(ox)_3]_n^{1n-}$ type nets, unipositive cations similar to the $[M^{II}(bpy)_3]^{2+}$ cations will be needed. The orthometalated rhodium compound $[Rh^{III}(ppy)_2(bpy)]^+$, where ppy is 2-phenylpyridine, is a valuable potential candidate. In a preliminary study using X-ray powder diffraction, we obtained positive results. Further experiments, including an X-ray structure determination, will be needed in order to fully describe that system. In a similar way, studies employing $[Cr(bpy)_3]^{3+}$ cations to build up $[M^{I}M^{II}(ox)_3]_n^{3n-}$ type nets will be undertaken.

With the aim of pursuing extended experiments in the field of magnetism, the $M^{II}M^{III}$ combination within the 3D net is of particular interest. It will offer an ordered, alternating 3D lattice with the attractive valence states II and III.

Another aspect of these systems not yet mentioned is that they can be used to study energy transfer reactions. By placing $[Ru(bpy)_3]^{2+}$ cations into the structurally well characterized vacancies of the nets and exciting these cations in their absorption bands, a diversity of deactivation processes in the function of the metal combination within the surrounding net can be observed. In this respect, a systematic study has also been started in order to elucidate the system's potentiality.

Acknowledgment. Gratitude is expressed to the Swiss National Science Foundation for financial support under Project No. 20-34063.92. The authors also thank Dr. M. Baumgartner, University of Zürich, for assistance with the metal analyses, Dr. Th. Kohlhaas, University of Mainz, for assistance in performing the magnetic susceptibility measurements, Dr. habil. H. Spiering, University of Mainz, for stimulating discussions, and Dr. A. Linden, University of Zürich, for helpfully reading the manuscript.

Supplementary Material Available: Tables of atomic fractional coordinates (Tables SI, SII, SIII), bond lengths and angles (Tables SIV, SV), and anisotropic displacement parameters (Tables SVI, SVII, SVIII) (9 pages); listing of observed and calculated structure factors (SIX, SX, SXI) (23 pages). This material is contained in many libraries on microfiche, immediately follows this article in the microfilm version of the journal, and can be ordered from the ACS; see any current masthead page for ordering information.